ACOUSTICS 2017 PERTH
SOUND, SCIENCE AND SOCIETY

Application of FAMPRADOP ("Far-range Analytical Model for the Pressure Radiated from a Driven Offshore Pile") to the far-range cases of the COMPILE 2014 Workshop

Marshall V. Hall

Kingsgrove, NSW Australia (retired)

ABSTRACT

The cases considered by the COMPILE 2014 workshop in Hamburg defined a pile (length 25 m), a shallow-water environment (depth 10 m), the pile's vertical position in it, and a force waveform on the pile head. It also defined both close-range and far-range receiver positions, at which acoustic Sound Exposure Levels (SEL) and Peak of the Sound Pressure Level (P-SPL) were to be calculated. The organisers published a comparison of results from six participants' pile vibration and far-range propagation models during 2016. Five were Finite-Element Models and one was a Finite-Difference Model; there was no analytical model. For far-ranges, the workshop nominated ranges of 0.75, 1.5, 10, 20 and 50 km. The writer's in-house analytical model FAMPRADOP ["Far-range Analytical Model for Pressure Radiated from a Driven Offshore Pile"] has recently been applied to the far-range COMPILE workshop cases. At 0.75 and 1.5 km, the six participants' results and FAMPRADOP agreed closely amongst each other. At the greater ranges, some participants' results differed from the others, by up to 15 dB at 50 km. The FAMPRADOP results generally lie close to the minimum of the spread in the participants' results, for reasons that will be discussed.

1 INTRODUCTION

For predicting underwater sound radiation from offshore pile-driving, it is expedient to separately discuss close-ranges (up to around 30 m) and far-ranges. At close ranges, the sound pressure is determined primarily by the pile vibration, and modelling published so far has either ignored the environment or approximated its effect by considering only one reflection by each of the sea surface and seabed. The most popular method used by vibration models is the numerical "Finite-element model" (FEM), and there are subtle differences amongst the different implementations that have been published.

At far-ranges, it is necessary to incorporate propagation models that can compute pressure at any horizontal range and receiver depth from an omnidirectional point source of unit strength. For shallow water, there are three types of models available: normal-mode (NM), wave-number integration (WNI), and parabolic equation (PE). NM and WNI models require that the sound source be represented by one or more omnidirectional point sources in a vertical line array (VLA), and the noise modeller's task is to define a VLA that is equivalent to the vibrating pile. PE models compute the propagated pressure using a marching algorithm, and can be started with a depth-profile of the sound-pressure at a close-range.

To compare the different models, the "COMPILE" benchmarking workshop was held in Hamburg Germany, during 2014 (Lippert, et al. 2016). The general case defined a single pile, a shallow-water environment, and the pile's vertical position in it. Rather than defining the components of a piledriver, a simple analytical (although reasonably representative) axial force waveform applied to the pile head was defined. Individual cases defined both close-range and far-range positions, at which acoustic Sound Exposure Level (SEL) and Peak of the magnitude of the Sound Pressure Level (P-SPL) were to be calculated. Seven groups of participants applied their pile-vibration models to the close-range cases, and a comparison of their results was published by the workshop organisers and participants (Lippert, et al. 2016). For the far-ranges (at least 750 m), six pile-vibration models were applied, of which five were Finite-Element Models (FEM) and one was a Finite-Difference Model (FDM); there was no analytical model. Only the FDM took account of negative feedback due to radiation loading (the reduction in vibration caused by the external and internal pressures created by the vibration); the FEMs simulated pile damping as being due entirely to viscous drag between the embedded pile segment and the seabed.

The workshop nominated receiver ranges of 0.75, 1.5, 10, 20 and 50 km. The six participant results for SEL and P-SPL agreed closely amongst each other at ranges up to 1.5 km. At greater ranges, some of the results were significantly different from the others, with the disparity reaching a maximum of 15 dB at 50 km.

Models of pile vibration generated using finite element models generally ignore radiation loading and consequently the axial phase velocity of the vibration waves is assumed to be the plate or bar velocity of the steel, with a very small intrinsic loss factor. If there is no other source of loss, the resulting pile vibration will produce "long ringing signals in the water column" (Lippert, et al. 2016), which is conceded to be unrealistic. Some models have assumed all the loss occurs in the embedded segment of the pile, due to drag imposed by a viscous seabed. This assumption predicts that radiated noise will decrease as a pile's embedment increases.

When radiation loading is considered (Hall 2015), the existence of vibration-produced radiation leads to a vibration phase velocity whose features include significant loss and dispersion. If loss in vibration (due to radiation) is combined with a small reflection loss at the toe (due to downward radiation into the seabed by the pile's annular under-surface), it appears to be unnecessary for a noise model to also include significant loss due to seabed viscosity.

Since the output parameters of current interest are P-SPL and SEL, it is worthwhile to consider their sensitivity to vibration of the embedded segment of a pile. The initial pulse of the radiated waveform is the waterborne Mach wave from the initial downward travelling vibration wave (Reinhall and Dahl 2011). This will have a higher P-SPL that any successive pulses that are (of necessity) due to vibration waves that have been reflected at the pile toe. P-SPL will therefore be independent of toe-reflectivity or seabed viscosity. The initial pulse will also contain most of the energy (Lippert, et al. 2016) (Reinhall and Dahl 2011). SEL will therefore be a slowly varying function of toe-reflectivity or seabed viscosity.

2 MODEL OF PILE VIBRATION

2.1 The COMPILE Scenario

The dimensions, pile elastic properties, and the environment of the COMPILE scenario are listed in Table I (Lippert, et al. 2016). A small value, comparable with the intrinsic loss in steel, is used for the Young Modulus Loss factor in the pile. The value of 0.101 presented by Lippert et al (2016) as the loss due to the effect of seabed viscosity on pile vibration is not used here. The bar and plate velocities (q_b and q_p) are derived from the pile material's Young Modulus, density and Poisson ratio (Y, ρ_s, and ν). The bar and plate ring frequencies (f_b and f_p) are derived from the bar and plate velocities respectively, as well as the pile wall mean radius (a).

Table 1: Pile dimensions, pile elastic properties, and the environment of the COMPILE scenario.

Parameter	Value
Pile wall mean radius, *a (m)*	0.975
Pile wall thickness (m)	0.05
Pile Length, *L* (m)	25
Pile Young's modulus, Y *(GPa)*	210
Pile Young Modulus loss factor	0.001
Pile density, ρ_s *(kg/m^3)*	7850
Pile Poisson ratio, ν	0.3
Pile's bar and plate velocities (m/s)	5172 and 5422
Pile's bar and plate ring frequencies (Hz)	844 and 885
Seafloor depth, D (m)	10
Seawater and seabed sound-speeds, (m/s)	1500 and 1800
Seawater and seabed densities (kg/m^3)	1025 and 2000
Seabed sound absorption coefficient (dB / λ)	0.469

For each pile segment (immersed and embedded) it was specified that the interior and exterior media are to be the same.

2.2 Damping of vibration waves along the pile

When considering pile vibration, FAMPRADOP does not incorporate the "equivalent damping values for the embedded part of the pile" provided with the cases to account for “losses induced by the interaction between the pile and the sediment” (Lippert, et al. 2016). Instead, "The reflectivities of the pile head and toe are assigned frequency-independent values of -1 and -0.8, respectively" (Hall 2015). These negative reflectivities applied to the radial displacement wave; the reflectivities of the axial displacement wave are both positive. It is appropriate here to comment on the following statement (Lippert, et al. 2016, 1062-1063):

> *The most significant damping effect in offshore impact pile driving results from the interaction between the embedded section of the pile and the surrounding sediment, both inside and outside the pile. A neglect of these damping effects has been observed to yield sharp resonances in the spectral density levels of the sound pressure and long ringing signals in the water column, which are unrealistic and not observed in measurement data; see, for example, Reinhall & Dahl (2011)*

If radiation loading is included then vibration in the immersed segment of a pile will decay ("dampen") regardless of any other loss factors. If the entire pile is in liquid, the pile would radiate sound and this radiation would be accompanied by significant loss of vibration energy over a wide frequency band. Thus, vibration waves decay even if a pile is entirely in an inviscid liquid. The damping rates for the immersed and embedded segments of the COMPILE pile (both “filled”) have been computed using the algorithm described in Hall (2015). The results are shown in Figure 1 by the blue and red curves (2 - immersed and 3 - embedded). The main peak at 700 Hz is related to the bar and plate ring (radial resonance) frequencies of the COMPILE pile (844 and 885 Hz); for axisymmetric vibration, there is only one bar ring frequency and one plate ring frequency. The cause of the damping shown in Figure 1 is the (inviscid) transfer of vibration energy into radiation energy.

Whereas the spectra of damping along a filled pile have multiple peaks, the spectra for an empty pile (computed but not shown) have only one peak each, at 760 Hz (segment 2) and 450 Hz (segment 3). The peaks in the spectra for a filled pile at frequencies above 1000 Hz are therefore due to the presence of a liquid interior medium.

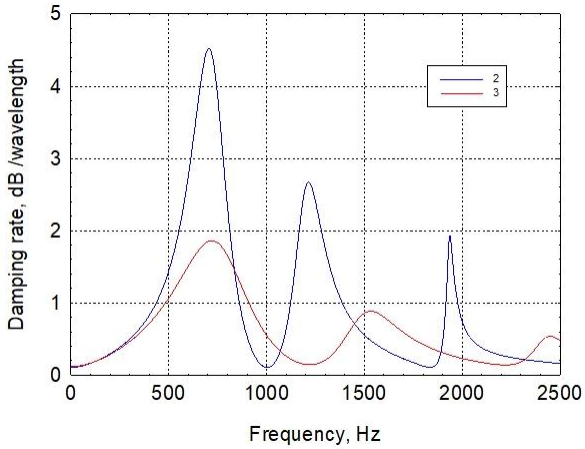

Figure 1: Theoretical damping rates along the filled pile assumed for the COMPILE workshop. In the legend, ‘2’ and ‘3’ refer to the immersed and embedded pile segments respectively.

2.3 Axial phase velocity

The phase velocities of the immersed and embedded segments of the COMPILE pile have been computed using the algorithm described in Hall (2015). They will be denoted by V_2 and V_3 respectively. Phase velocity depends on all the parameters listed in Table I, except pile length. The results are shown by the blue and red curves in Figure 2. As prescribed, the internal medium of each pile segment is the same as the external medium (Lippert, et al. 2016). It is this feature that gives rise to the multiple peaks and troughs in the curves. The additional peaks for the “filled” pile are due to resonances between the internal liquid and the pile. The embedded curve has similar features to the immersed curve, but the maxima and minima caused by the (different) internal media occur at somewhat different frequencies.

Results for an empty pile (computed but not shown) have only one minimum and one maximum each, at 420 and 1100 Hz respectively (segment 2), and at 170 and 1280 Hz respectively (segment 3). The VLF and VHF limits of both V_2 and V_3 for an empty pile are the steel's bar and plate velocities (5172 and 5422 m/s).

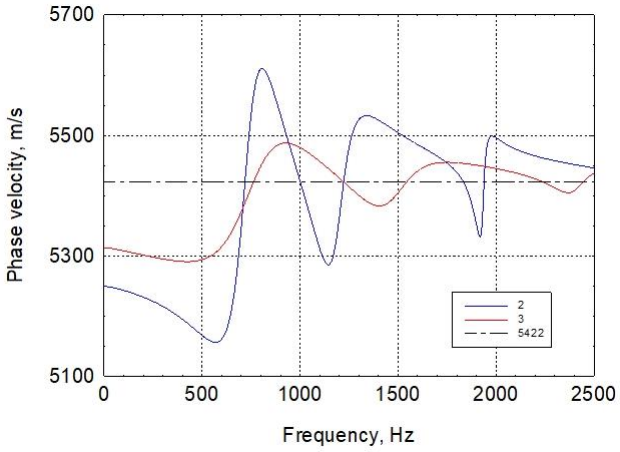

Figure 2: Real part of the Phase Velocity along the filled pile assumed for the COMPILE workshop. In the legend, '5422' represents the pile plate velocity.

3 METHOD FOR COMPUTING FAR-RANGE RADIATED SOUND

3.1 Exact (All-field) and approximate far-field radiation theories

In the "Transform Formulation of the Pressure Field of Cylindrical Radiators" (Junger and Feit 1993, 173-176) , a cylinder of finite length is represented as a Fourier Transform of a function of axial wavenumber. The Fourier Transform (FT) components may be considered as virtual cylindrical shells of infinite length, but with different axial vibration wavenumbers (equivalent to a temporal transient being represented as an FT of a function of frequency, whose virtual oscillations last forever). The formulation as presented assumes the external medium to be an unbounded homogeneous fluid. It consists of both an exact radiation model (valid for both the near-field and far-field) and a far-field approximate model.

The "Stationary-Phase Approximation to the Far-Field of Cylindrical Radiators" is applicable, subject to two caveats:

[1] the horizontal range is so large that the Hankel function, whose argument is (horizontal wavenumber × horizontal range), may be replaced by its asymptotic expression over the whole frequency band that affects the result. The integrand in the IFT, a function of vertical (axial) wavenumber (γ), then has a single point of stationary phase at $\gamma = k\cos\theta$. This corresponds to the origin (the pile at the sea surface, $r = 0,\ z = 0$) being the main contributor to the radiated noise.

[2] the requirement that the major source of noise at the receiver be at the origin implies that no vibration wave along the pile can be the major component of the signal. Thus, the major contribution at a receiver cannot be a Mach wave. Since a Mach wave is a characteristic feature of pile-driving noise, the stationary phase approximation may potentially be in significant error. It will be seen later however that FAMPRADOP does produce a reasonable estimate for the Mach wave.

If these two conditions are met, the IFT integral over γ may be approximated using the method of stationary phase. Whereas the exact model is conveniently expressed in cylindrical coordinates (horizontal range r and receiver depth ζ), the stationary phase expression is more conveniently presented in spherical coordinates:

$$R = \sqrt{r^2 + \zeta^2} \quad \text{and} \quad \theta = atan(r/\zeta) \tag{1}$$

where R is slant range and θ is colatitude. The result for the harmonic SPL (Junger and Feit 1993, 176), but simplified for axial symmetry and adapted to a time dependence of $\exp(+i\omega t)$, is:

$$P(R,\theta,\omega) = \frac{-i\omega^2 \rho\, \widehat{W}(k\cos\theta)}{\pi\, k \sin\theta\, H_1^{(2)}(ka\sin\theta)} \frac{e^{-ikR}}{R} \quad (2)$$

where

$$\widehat{W}(k\cos\theta) = \int_0^L W(z)\, exp(i\, k\cos\theta\, z)\, dz \quad (3)$$

and $H_1^{(2)}$ is the Hankel function of the second kind and order 1. It follows from Eq. (2) that the phase of *P* is the phase of the straight ray from origin to receiver. An axisymmetric harmonic force (of angular frequency $\omega = 2\pi f$) acting on a pile head will cause an "initial" harmonic axial displacement wave to travel down a pile (toward increasing z). "Initial" here means unaffected by subsequent toe reflections. The axial displacement in the immersed pile segment may be expressed as:

$$U(z) = U_0 e^{-i\omega z/V_2} \quad (4)$$

where V_2 is the (frequency-dependent) phase velocity in the immersed segment and U_0 is the "initial" axial displacement at the sea surface ($z = 0$). The axial and radial displacements are each the sum of the initial component and an infinite sequence of reflections, and the radial displacement $W(z)$ may be expressed as:

$$W_2(z) = \chi_2 U_0 \frac{e^{-i\omega z/V_2} - 0.8e^{-i\omega(2L-z)/V_2} e^{-2i\omega(L-D)/V_3}}{1-0.8e^{-2i\omega T}}, 0 < z < D \quad (5)$$

$$W_3(z) = \chi_3 U_0 e^{-i\omega D/V_2} \frac{e^{-i\omega(z-D)/V_3} - 0.8e^{-i\omega(2L-z)/V_3}}{1-0.8e^{-2i\omega T}}, D < z < L \quad (6)$$

where $\chi_n = W_n/U_n$ is a depth-independent ratio, given by either Eq. (II.4) in Junger and Rosato (1954), or Eqs. (14) and (19) in Hall (2015), and T is the one-way travel time from head to toe:

$$T = H/V_1 + D/V_2 + (L - D - H)/V_3, \quad (7)$$

in which H is the height of the head above the sea surface, and the suffixes 1, 2 and 3 refer to the aerial, immersed and embedded pile segments, respectively. Since the COMPILE case placed the pile head at the sea surface, $H = 0$.

One practical outcome of the results for V_2 and V_3 shown in Figure 2 is the fundamental frequency of the pile's longitudinal oscillation, the reciprocal of double the travel time given by Eq. (7). Considering the curves at frequencies up to a few hundred Hz, $V_2 \sim 5250$ m/s and $V_3 \sim 5300$ m/s, so $2T \sim 2(10/5250 + 15/5300) = 0.0095\ s$. The fundamental longitudinal frequency of the COMPILE pile therefore should be approximately 105 Hz.

3.2 Axial displacement caused by an imposed Force

It has been shown (Hall 2017) that, in terms of an imposed harmonic axial force F, the initial axial displacement at the head is given by:

$$U_0 = U'(0)\ V_n/(-i\omega) = F/(i\omega\, A\, \rho_s V_n) \quad (8)$$

where A is the cross-sectional area to which F is applied (the cross-sectional area of the pile), the depth-derivative U' is the axial strain, and suffix n corresponds to the medium immediately below the pile head; $n = 1$ for the usual exposed head ($H > 0$), but $n = 2$ for COMPILE ($H = 0$). When the FT of an imposed transient force waveform is taken, yielding $F(\omega)$, Eq. (8) will provide the connection between that force and the consequent axial displacement of the head. The radial displacement is then obtained using χ_2.

4 FAMPRADOP

In broad terms, FAMPRADOP is similar to the models used by some of the workshop participants, in that it computes the (complex) source strengths of a VLA of point sources. It yields results (only) at far-ranges, and therefore differs fundamentally from the close-range model described by Hall (2015). FAMPRADOP is based on the Membrane thin-shell vibration theory (Leissa 1993, 37).

4.1 Pile as sum of contiguous (λ/2) tubular layers

Before presenting expressions for point sources, let us consider the pile as the sum of several contiguous tubular layers, each a half-wavelength thick: $\delta = \lambda/2$. The number of immersed layers is $N = int(2D/\lambda)$. The upper face of the j'th layer is at depth $z_j = (j-1)\,\lambda/2$, and the colatitude of a receiver at (r, ζ) measured from the layer's upper face is $\theta_j = atan\left[r/\left(\zeta - z_j\right)\right]$. For each tubular layer, the origin for colatitudes is the centre of the layer's upper face. Except at frequencies below the pile's fundamental longitudinal frequency of 105 Hz (where the radiated noise is negligible), the thickness (tallness) of each layer is small in relation to the range to a receiver. The major noise source may thus be assumed to be the layer's upper surface (as distinct from a point between the upper and lower surfaces). In this case, the stationary phase approximation will be valid, and Eq. (2) may be used for each layer. The (additional) assumption that the total radiated harmonic pressure $P(\omega)$ at the receiver (R, θ) is the coherent sum of the N individual signals then yields:

$$P(R,\theta,\omega) = \frac{-i\omega^2\rho}{\pi k}\sum_{j=1}^{N}\frac{\widehat{W}_j(k\cos\theta_j)}{\sin\theta_j\, H_1^{(2)}(ka\sin\theta_j)}\frac{e^{-ikR_j}}{R_j} \tag{9}$$

Since the elastic properties of each layer are the same as its neighbours, there is no reflection at the horizontal surfaces of any layer, other than those at the surface and seafloor. The dependence of radial displacement on depth within layer j may therefore be expressed as:

$$W_{j2}(z) = W\left(z_j\right) exp(-i\omega\, z/V_2)$$

in which z is depth below z_j. The γ-Fourier Transform of W_j, $\widehat{W}_j\left(k\cos\theta_j\right)$ is therefore given by:

$$\widehat{W}_j\left(k\cos\theta_j\right) = W\left(z_j\right)\int_0^{\delta} exp\left(-i\omega\, z/V_2 + ik\cos\theta_j\, z\right) dz = W\left(z_j\right)\,\delta\, e^{i\varphi_j}\sin\varphi_j/\varphi_j \tag{10}$$

where

$$\varphi_j = k\left(\cos\theta_j - c/V_2\right)\delta/2 \tag{11}$$

In Eqs. (10) and (11), the dependence on colatitude is the same as the shape of the beam from a continuous line source, steered in the direction of $\theta_M = \mathrm{acos}[Real(c/V_2)]$, the angle of the Mach wave. At the complex colatitude $\theta_M^c = \mathrm{acos}(c/V_2) = (74.1, 0.12)°$, φ_j would be exactly zero. It has been found that with each colatitude set to the Mach colatitude, Eq. (9) yields a good approximation for the pressure of the Mach wave from the entire pile.

4.2 An equivalent VLA of point sources

In Eq. (9), if the expression that is a function of colatitude were a constant then the pressure could be regarded as due to N equal point sources. A VLA of N point sources with a spacing of a half-wavelength generally has a beam pattern similar to that of a line source of the same length (Urick 1983, 57,59). The number of sources will be proportional to frequency. The equivalence of the line and VLA sources is illustrated in Figure 3 for the frequency of 2000 Hz, where there are 26 point-sources in a length of 10 m. Both line and VLA sources are steered in the direction of 73° from the pile axis, to be consistent with the angle of the Mach wave emitted by a steel pile in seawater (Reinhall and Dahl 2011) (Hall 2015). The approximation is very good for colatitudes from 50° to around 95°, an interval that should suffice to cover the angles involved in far-range sound propagation

(contributions travelling at steep angles attenuate more rapidly than do shallow-angle contributions). The growing deviation in phase between the two curves is due in part to the continuous line being able to use a precise value for the ratio $2L/\lambda$, whereas the corresponding ratio for the VLA is constrained to be an integer. These calculations have been repeated for the pile's fundamental frequency (105 Hz), for which it is found that the validity domain of the approximation is much smaller; from around 63° to 83°. Nevertheless, this interval should suffice to cover most of the angles involved in far-range sound propagation.

To convert Eq. (9) to an expression suitable for a VLA of point sources, their source strengths must be angle-independent, so a suitable fixed value for θ_j must be selected. The source strength of source j will be the combination of factors in Eq. (9) that multiplies the factor e^{-ikR_j}/R_j. The sensitivity of the results to θ_j was determined by computing SEL(spectrum) (at range 10 km, depth 1 m) for $Real(\theta_j)$ ranging from 0° to 90°. "SEL(spectrum)" denotes the area under the square of the Pressure-magnitude spectrum $|P(f)|^2$; the details of the algorithm used are described later. The results vary by less than 1 dB for angles between 60° and 90°, so the complex Mach angle θ_M^c was selected (the resulting SEL is slightly above the curve based on real angles). θ_M^c varies with frequency (because V does), and its value at 2 kHz is $(74.1, 0.12)°$. For the source strengths of the point sources, Eq. (9) for the tubular layers will therefore be used, except that the colatitude-dependent factors will be replaced by their values at θ_M^c.

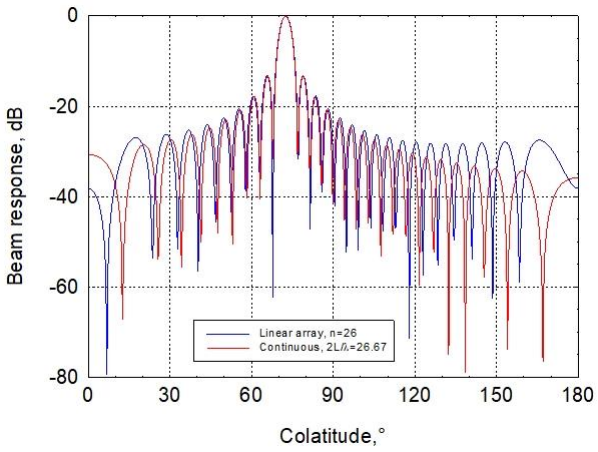

Figure 3: Far-field beam patterns at 2000 Hz of a continuous 10-m line and a VLA of the same length with half-wavelength spacing. Both sources are steered in the direction of 73° from the pile axis.

The COMPILE workshop specified a Nyquist frequency (half the sampling rate) of 2500 Hz. Since the FFT routine used (Ferziger 1998) requires the number of samples to be an integer power of 2, the time windows to be used were adjusted accordingly.

One issue to address is whether the embedded pile segment needs to be included in the calculation. The loss per wavelength travelled by sub-bottom sound radiation is of the order of 1 dB /λ (Hamilton 1980). At frequencies of the pile's fundamental frequency (105 Hz) or more, the wavelength of sound waves in unconsolidated seabed will be no more than 20 m, and thus sub-bottom propagation to a range of the order of 1 km will dampen by at least 50 dB. Since the wavelengths of shear waves are around half those of sound waves (at most), shear waves will dampen by at least 100 dB. This means that the sub-bottom propagated signals will be negligible in relation to the waterborne propagated signals at frequencies above around 100 Hz. In summary: although sub-bottom propagation may suffer little loss at low frequencies, this is of no consequence since the spectrum of pile driving noise below the fundamental frequency is small in relation to the spectrum at higher frequencies. Since the contribution of sub-bottom sources will be insignificant at far-ranges, only the point sources in the water will be included.

4.3 Spectra of the radiated sound

At any frequency, source depth, receiver range, receiver depth and environment, propagation models generally report the pressure magnitude. Some also report the complex pressure. These models assume the source to be a point source with unit "strength"; the latter meaning that the pressure magnitude is unity at unit distance from the source (spherical spreading is accurate at such a short distance, unless the source is very close to a reflecting surface). The results for pressure magnitude are converted to decibels and described as "Transmission (or

Propagation) Loss". In this paper, the results for complex pressure will be referred to as "Normalised Complex Pressure", since they are normalized to unity at unit distance.
At each frequency to be used in the current analyses, the complex harmonic source strengths are multiplied by the normalized complex pressures computed by the ORCA propagation model (Westwood, Tindle and Chapman 1996) for each of N source depths. Since ORCA assumes a time dependence of $e^{-i\omega t}$, the complex conjugates of those results are used. The products are the harmonic pressures at far ranges. The N complex pressures at the receiver from the N sources were summed coherently, yielding the FT of the received pressure. Spectra computed with FAMPRADOP for the COMPILE scenario with a receiver at 1-m depth and horizontal ranges of 0.75, 1.5, 10, 20 and 50 km are shown in Figure 4. The frequency resolution (pixel) decreases from $1/3.3 = 0.3\ Hz$ at 0.75 km to $1/100 = 0.01\ Hz$ at 50 km (these resolutions were found to be required for the respective inverse-FTs that will be described later). The fundamental frequency of 105 Hz and four of its overtones are evident. Also evident is the rapid fall-off in the spectrum below around 300 Hz as the range increases (the COMPILE scenario's cut-off frequency for modal propagation is 68 Hz).

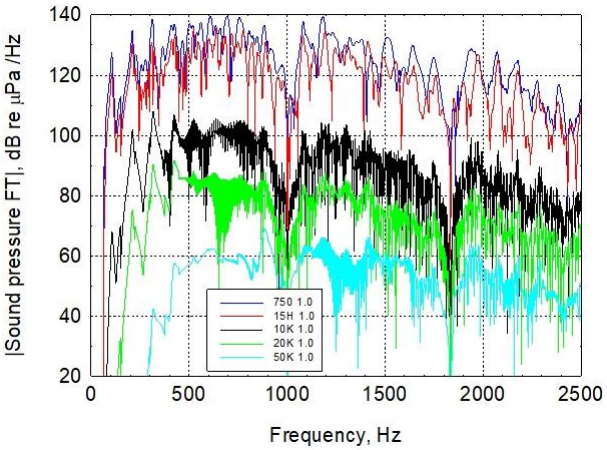

Figure 4: Sound pressure spectra computed with FAMPRADOP for the COMPILE scenario with a receiver at 1-m depth and horizontal ranges of 0.75, 1.5, 10, 20 and 50 km.

4.4 Waveforms of the radiated sound

The FTs were inverted to obtain waveforms. The number of frequencies (NUMFREQ) for the FFT was successively doubled, until the resulting waveforms stabilised. At 0.75 km, the values required ranged from 2^{13} to 2^{15}, whereas at 50 km they ranged from 2^{18} to 2^{20}. As an illustrative example, four sound pressure waveforms computed with FAMPRADOP for the COMPILE scenario with a receiver at 10-km horizontal range and 1-m depth are shown in Figure 5. The sizes of the FTs that produced these four waveforms are 2^{15}, 2^{16}, 2^{17} and 2^{18} (the corresponding time windows are = 6.5, 13, 26 and 52 s). Although the abscissa label is "Time" it should not be interpreted as travel time; the time computed by FAMPRADOP is 1.2 s, whereas the actual travel time would be approximately 6.7 s (the reason for this error is unknown).

The reassuring aspect of the waveforms in Figure 5 is that as NUMFREQ (and time window) increases, the imaginary parts decrease and the peaks of the real parts asymptote to a value that can be estimated with a small uncertainty. SEL(spectrum) is constant at 129.7 dB re µPa^2.s, and the four successive values of SEL(real waveform) are less than SEL(spectrum) by 1.61, 0.39, 0.095, and 0.024 dB respectively. "SEL(real waveform)" denotes the integral over the time window of the square of the real part of the waveform. It is interesting that each time NUMFREQ is doubled, the error in SEL(real waveform) reduces to around 25% of its previous value.

4.5 Far-range SEL and P-SPL

Participants' results for SEL and P-SPL at receiver depths of 1 and 9 m have been published (Lippert, et al. 2016), and those at 1 m have been read off for presentation in Figures 6 and 7 (the 9-m results were found to yield similar comparisons). The spread of the participants' results at each range is indicated by an error bar. FAMPRADOP computed two measures of SEL, "SEL(spectrum)" and "SEL(real waveform)". The latter increases with NUMFREQ (accompanied by a reduction in the imaginary part of the waveform) and asymptotes to SEL(spectrum). The successive doubling of NUMFREQ was continued until SEL(real waveform) had risen to within 0.1 dB of SEL(spectrum). NUMFREQ was then doubled once more so that the variability in P-SPL could be examined.

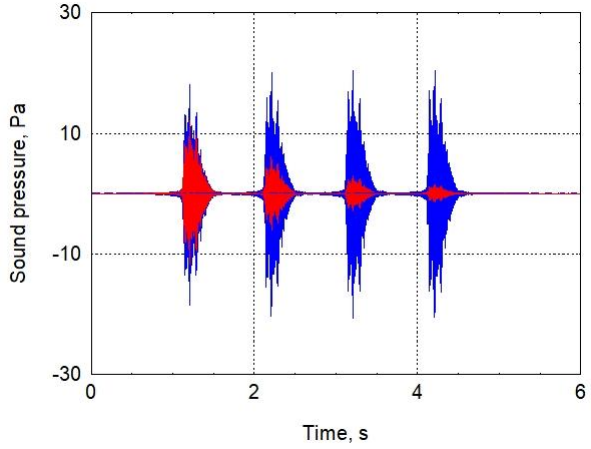

Figure 5: Sound pressure waveforms computed with FAMPRADOP for the COMPILE scenario with a receiver at 10-km horizontal range and 1-m depth, using four time-windows from 6 to 52 s. KEY: Blue: real part, Red: imaginary part. The first waveform is presented at the time computed by FAMPRADOP (1.2 s); the other three are successively shifted by 1 s for clarity.

The participants' and FAMPRADOP far-range results for SEL at a receiver depth of 1 m are compared in Figure 6. The slightly different values for the two FAMPRADOP SELs are not shown individually. At 0.75 and 1.5 km the differences are negligible, whereas from 10 km to 50 km the FAMPRADOP results lie at or near the minima of the spreads in the participants' results.

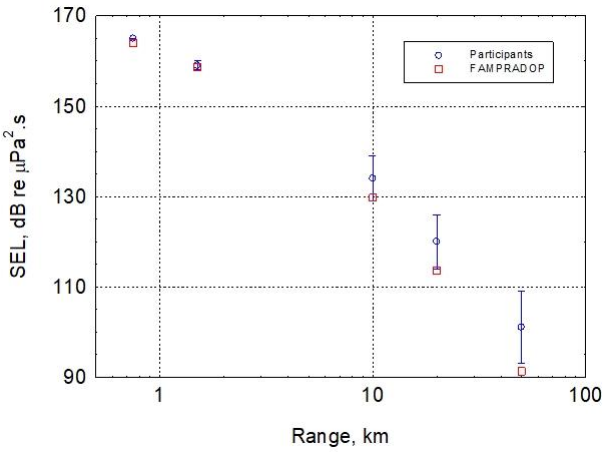

Figure 6: Comparison of far-range results for SEL at a receiver depth of 1 m.

The participants' and FAMPRADOP far-range results for P-SPL at a receiver depth of 1 m are compared in Figure 7. The FAMPRADOP results lie between the minimum and median of the distributions of the participants' results. The variability in the FAMPRADOP results is generally of the order of ±0.01 dB.

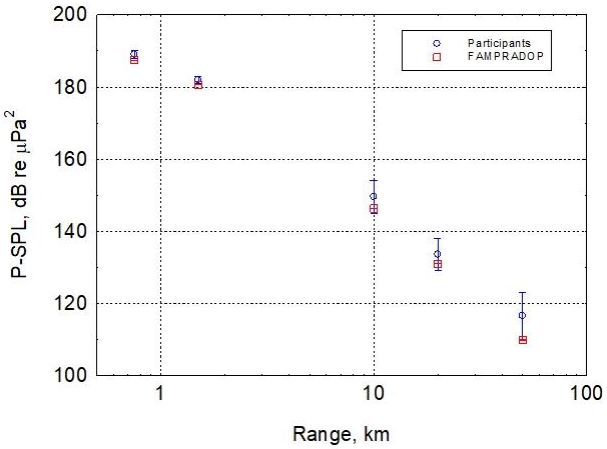

Figure 7: Comparison of far-range results for P-SPL at a receiver depth of 1 m.

5 CONCLUSIONS

At the shorter ranges (0.75 and 1.5 km) the spread in the results for both SEL and P-SPL are small, and FAMPRADOP results are close to the participants'.

At the longer ranges (10, 20 and 50 km), the spread in the participants' SEL results increases with range from ± 5 dB to ± 8 dB. The spread in the participants' P-SPL results increases with range from ± 4 dB to ± 7 dB.

For SEL at 1 m depth, the FAMPRADOP results lie at or near the minimum of the spread in the participants' results. For SEL at 9 m depth, the FAMPRADOP results lie at the median at 10-km range, but decrease to the minimum at 50 km.

For P-SPL at 1 m depth, the FAMPRADOP results lie between the minimum and median of the participants' spreads at 10 and 20 km, and at the minimum at 50 km. For P-SPL at 9 m depth, the spreads are small except at 50 km. The FAMPRADOP results are close to the participants' results at 10 and 20 km, but decrease to the minima at 50 km.

A conceivable reason for FAMPRADOP to (relatively) underestimate SEL and P-SPL by several decibels at ranges beyond 10 km is that the number of point sources (2 per wavelength) it uses is insufficient (one participant used a minimum of 5 sources). One would expect however that an inadequate number of sources would cause a similar shortfall at all ranges, including 0.75 and 1.5 km.

REFERENCES

Ferziger, Joel H. 1998. *Numerical methods for engineering applications.* 2nd. Wiley.

Hall, Marshall V. 2017. "Accuracy of the Far-Field Approximation for the Underwater Sound Radiated When Immersed Steel and Lead Piles (with Non-reflective Toes) are Driven by a Harmonic Axisymmetric Force." *Acoustics Australia.* doi:10.1007/s40857-017-0096-5.

Hall, Marshall V. 2015. "An analytical model for the underwater sound pressure waveforms radiated when an offshore pile is driven." *The Journal of the Acoustical Society of America* 138: 795–806.

Hamilton, Edwin L. 1980. "Geoacoustic modeling of the sea floor." *The Journal of the Acoustical Society of America* 68: 1313-1340.

Junger, Miguel C, and David Feit. 1993. *Sound, Structures and Their Interaction.* New York: Acoustical Society of America.

Junger, Miguel C, and Frank J Rosato. 1954. "The Propagation of Elastic Waves in Thin-Walled Cylindrical Shells." *The Journal of the Acoustical Society of America* 26: 709–713.

Leissa, Arthur. 1993. *Vibration of shells.* New York: Acoustical Society of America.

Lippert, S, M Nijhof, T Lippert, D Wilkes, A Gavrilov, K Heitmann, M Ruhnau, et al. 2016. "COMPILE—A Generic Benchmark Case for Predictions of Marine Pile-Driving Noise." *IEEE Journal of Oceanic Engineering* 41 (4): 1061-1071.

Reinhall, Per, and Peter H Dahl. 2011. "Underwater Mach wave radiation from impact pile driving: Theory and observation." *The Journal of the Acoustical Society of America* 130: 1209–1216.

Urick, Robert J. 1983. *Principles of Underwater Sound.* 3rd. New York: McGraw-Hill Book Company.

Westwood, Evan K, Chris T Tindle, and N. Ross Chapman. 1996. "A normal mode model for acousto-elastic ocean environments." *The Journal of the Acoustical Society of America* 100: 3631–3645.